This document is the accepted manuscript version of the following article: Iannarelli, R., Ludwig, C., & Rossi, M. J. (2022). The kinetics of adsorption and desorption of selected semivolatile hydrocarbons and H2O vapor on two mineral dust materials: a molecular view. Journal of Physical Chemistry A, 126(46), 8711-8726. https://doi.org/10.1021/acs.jpca.2c04903

The Kinetics of Adsorption/Desorption of selected semivolatile Hydrocarbons and H_2O Vapor on two Mineral Dust Materials: a molecular View

Riccardo Iannarelli[1], Christian Ludwig[2,3] and Michel J. Rossi*[3]

[1] École Polytechnique Fédérale de Lausanne (EPFL), Risk Prevention, EPFL VPO-SE OHS-PR, Station 6, CH-1015 Lausanne, Switzerland ; riccardo.iannarelli@gmail.com

[2] Paul Scherrer Institute (PSI), ENE LBK CPM, CH-5232 Villigen PSI, Switzerland; christian.ludwig@epfl.ch; christian.ludwig@psi.ch

[3] École Polytechnique Fédérale de Lausanne (EPFL), ENAC IIE GR-LUD, Station 6, CH B2 397, CH-1015 Lausanne, Switzerland ; michel.rossi@epfl.ch

ABSTRACT

A flowing gas experiment using a Knudsen flow reactor was performed on a series of seven semivolatile probe gases interacting with two often used mineral dust materials, namely Arizona Test Dust-Coarse (ATD) and Kaolinite. The used semivolatile probe gases were applinate (acetate ester), pipol (ethylester of 2-methylvaleric acid), benzylacetate (acetate ester of benzylalcohol), menthol (alcohol), toluene, limonene and γ-terpinene (terpene hydrocarbons). Uptake experiments under molecular flow conditions resulted in absolute coverages and initial uptake coefficients γ_0 based on the geometric sample surface. Integration of a simple Langmuir adsorption model afforded an analytical solution of the desorption kinetics of the semivolatile hydrocarbon upon spontaneous desorption from the solid mineral dust substrate at ambient temperature. Numerical fitting of the desorption rate resulted in adsorption (k_a) and desorption (k_d) rate constants where $1/k_d$ represented the surface residence time of the adsorbed semivolatile. The major conclusions are: (a) Desorption at short ("prompt") and long time scales reveal stronger binding to ATD compared to Kaolinite for all tested organic probe gases; (b) No difference of desorption yields and kinetics was observed for H_2O vapor on both substrates; (c) Prompt desorption at ambient temperature starts with the immediate detection of probe gases adsorbed on the vessel walls of the sample compartment followed by the slower rise and decay of semivolatiles adsorbed on the substrate leading to k_a and k_d; (d) Surface residence times at ambient temperatures for semivolatile organics vary from 50 to 40'000 s for toluene/ATD to menthol/ATD, respectively. For H_2O vapor 3000 s was measured on both Kaolinite and ATD; (e) Large initial uptake coefficients γ_0 in the range 0.25 to 0.77 were measured for all semivolatiles except for toluene whose values were roughly lower by one order of magnitude. Rapid saturation was observed in all cases except for limonene that appeared to undergo a chemical reaction on both mineral substrates.

[1] Left EPFL on October 31 2022. ORCID ID: 0000-0002-6185-6975

[2] ORCID ID: 0000-0002-0718-8195 is associated with the email address at PSI (christian.ludwig@psi.ch)

[3] ORCID ID: 0000-0003-3504-695X

1. Introduction

Mineral dust aerosol is the most prevalent type of atmospheric aerosol with an annual emission rate of 1600 Tg/a. This represents by far the highest emission rate of an aerosol on a global scale, by far more important than global primary and secondary organic aerosol (SOA) emission. [1] There are quite a number of scientific reviews dealing with this subject from the point of view of how atmospheric dust aerosol interacts with atmospheric gaseous components from a chemical-kinetics point of view. Examples of gaseous species include atmospheric oxidizers such as O_3, NO_2, $OH^\bullet$, $HO_2^\bullet$, $NO_3^\bullet$, as well as other reactive gases such as CO, CH_2O, SO_2, NH_3 and atmospheric acids such as HNO_3, HONO, H_2SO_4, carboxylic and dicarboxylic organic acids and the like. [2-4] In contrast, there are only a handful of studies describing the elementary multiphase chemistry of organic, mostly semivolatile organic compounds, in the presence of atmospheric dust aerosol particles. The present contribution is seen as closing a gap in the chemical-kinetic literature on semivolatile compounds interacting with the interface of refractory inorganic metal oxides and mineral dust materials. In contrast to the majority of reviews, three of which are listed above, the emphasis of this work is placed upon the change of the physical and chemical properties of the mineral dust interface in the aftermath of adsorption/desorption/reaction processes of semivolatiles with the original interface of mineral dust materials. The expected chemical change of the mineral dust interface may have consequences with respect to formation of secondary organic aerosols (SOA) originating from (photo-)chemical processing and ensuing multiphase chemistry as well as its mode of nucleation in the presence of organic compounds adsorbed on mineral dust. [5] A fact that suggests the importance of the interaction of mineral dust with semivolatile organics is that the global emission of organic aerosols amounts to 200 Tg/a whereas organic material is found in 20 to 60% in midlatitude continental, and in tropical forested areas in even 90% of all aerosols. [6, 7] Globally, most fine and ultrafine (long-lived) aerosol particles contain organic material despite the overwhelming source term of mineral dust. [8, 9]

In what follows we will briefly present a few pertinent examples from the literature regarding the chemical kinetics of multiphase chemistry of polyatomic organic molecules with the interface of either natural mineral dust materials or their proxies. It should be noted that the notion of “proxy” is neither reasonable nor applicable to substrates of complex interfaces as each member of the series possesses its own set of characteristic parameters that may not be generalized once on delves into the chemical kinetic details such as the lifetime of the adsorbate, the extent of coverage or the uptake/desorption kinetics. Two of the early publications on the interaction of organics on mineral dust proxies are the studies of Li et al. [10] and of Carlos-Cuellar et al. [11] that are reviewed by Usher et al. [2] In Li et al. acetaldehyde, acetone and propionic aldehyde interacted with SiO_2, α-Al_2O_3, TiO_2 and α-Fe_2O_3 (hematite) and CaO using the spectroscopic technique of diffuse reflectance both in the UV (200 to 400 nm) and in the mid-IR region (4000-1000 cm^{-1}). [10] The uptake and reaction kinetics of the adsorbates were studied using a Knudsen flow reactor (KFR) coupled to residual gas analysis. SiO_2 substrates only weakly and reversibly adsorbed the organics whereas aldol condensation reactions were observed on all studied oxide particles with basic and acidic properties. The self-coupling aldol condensation reactions showed a second-order rate dependence on the adsorbate after an induction period consistent with a Langmuir-Hinshelwood (LH) mechanism. [12, 13] Unfortunately, the quantitative evaluation is hampered by the fact that the adsorption has not been conducted to complete saturation. The same holds for the study of Carlos-Cuellar et al. [11] who focused on the kinetics of uptake of acetic acid, formaldehyde and methanol on the oxide interfaces of α-Fe_2O_3, α-Al_2O_3, SiO_2 using the KFR technique. A fast uptake was observed for acetic acid in contrast to SiO_2 where the extent of uptake was on the order of 1%. In addition, desorption of the organics occurred in the range of 50-100% for SiO_2 whereas on α-Fe_2O_3 and α-Al_2O_3 the desorption ranged from <1 to

15%. However, the observation times of adsorption onto the mineral oxide substrates were quite short, between 200 to 500 s, thus precluding saturation of adsorption and evaluation of total adsorption capacity in terms of a molecular monolayer.

Considering acetic acid and a natural mineral dust sample from the Gobi desert as an example Wang et al. [14] came to the conclusion that there are a plethora of different adsorption sites, especially in the presence of atmospheric water. Using a simple breakthrough experiment coupled to gas phase acetic acid detection using FTIR absorption total adsorption at saturation corresponded to a molecular monolayer in the absence of H_2O vapor (2.7 10^{14} molecule cm^{-2}). This amount was distributed among a reversible fraction that spontaneously desorbed (8.0 10^{13} molecule cm^{-2}) and a larger fraction that remained on the substrate (1.9 10^{13} molecule cm^{-2}). At 20% rh of the carrier gas a significant fraction of the irreversibly adsorbed acetic acid desorbed upon pumping owing to a displacement mechanism that replaced adsorbed acetic acid by water molecules in a competitive adsorption process thus releasing acetic acid into the gas phase. This example goes to show that in order to obtain predictive and realistic values based on laboratory experimental results that are applicable to atmospheric conditions one must undertake additional experiments beyond simple single gas experiments in order to capture the full gamut of reactive possibilities of a chemical multiphase system in the atmosphere. [15] H_2O is the most important interfering atmospheric gas affecting molecular adsorption/desorption processes, and examples abound demonstrating in general negative and sometimes also positive dependences of adsorption rate constants or uptake coefficients in the presence of atmospheric H_2O (See for example Figures 5, 8 and 18 of Tang et al. [3] reporting work on $OH^{\bullet}$ and H_2O_2 by Bedjanian et al. [16]; Pradhan et al. [17]; Wang et al. [18], Romanias et al. [19, 20]; El Zein et al. [21]).

Noteworthy is an experiment performed by Romanias et al. [22] using multidiagnostic detection in which the adsorbate was monitored using diffuse reflectance FTIR and the gas phase by Selected Ion Flow Tube Chemical Ionization MS (SIFT-MS). Limonene and toluene were chosen as gas phase semivolatile probe gases using NO^+ and H_3O^+ ions as ionizing gases through complex formation with the parent neutral gas, respectively. Saharan sand as well as deposited airborne dust from the Cap Verde Islands were used as reactive substrate. In addition to the interesting cross-calibration aspect between the quantitative SIFT-MS gas phase data and the diffuse reflectance FTIR integrated area pertaining to the molecular adsorbate the study highlights the significant difference of the reactivity of both limonene and toluene on Saharan sand as a function of SiO_2 (quartz) content: limonene seems to be bound more strongly on sands originating from areas of lower content in SiO_2 consistent with the fact that SiO_2 binds probe gases less strongly and more reversibly as it functions more like an inert filler in a composite mineral sample. The largest surprise in this work lies in the significantly different behavior of toluene and limonene as far as reversibility of adsorption is concerned: averaged across six different Saharan sand samples limonene desorbs much less readily than toluene whose reversibility is consistently higher throughout all examined samples. This behavior of limonene may be explained either by reactive adsorption converting limonene into a reaction product or by formation of a strongly bound adsorbate that does not spontaneously desorb at ambient temperature when reactive gas flow is interrupted. No known (measured) experimental parameters would have allowed to arrive at these conclusions from first principles comparing two unsaturated probe gases.

A relatively new aspect of studying the chemical kinetics of reactions on or in the presence of aerosol interfaces is represented by numerical electronic structure calculations using quantum chemical methods. [23] The goal of these studies is the investigation of accretion (dimerization) reactions on the interface of model or surrogate mineral dust substrates, for instance represented by silicic or trisilicic

acid simulating quartz and feldspars. Accretion reactions are closed-shell processes, have high barriers and are therefore good candidates for searching a catalytic activity on mineral dust surfaces. Examples for accretion reactions that have been examined are the addition of formic acid to formaldehyde (CH_2O), addition of H_2O to formaldehde to yield the gem-diol of formaldehde and the aldol condensation of methanol with formic acid. Although reaction barriers are lowered at the interface no convincing example of rate acceleration on mineral dust model substrates has emerged so far. Moreover, the interaction of semivolatile organic compounds with mineral dust materials has been found to be a potent generator of Reactive Oxygen Species (ROS) under atmospheric conditions containing free radicals and their precursors in the presence of atmospheric waters raising well-founded concerns about public health in dust episodes. [24, 25]

Therefore we have embarked on an effort to quantitatively compare seven different organic probe gases interacting with two different mineral dust materials that have been used repeatedly throughout the literature, namely natural low-ordered (LO) Kaolinite and coarse Arizona Test Dust (ATD-C) in an effort to screen basic molecular parameters such as uptake in terms of molecular adsorbed monolayers, adsorption rate constants and initial uptake coefficients on dry (H_2O-free) mineral dust substrates as well as desorption rate constants leading to surface residence times of adsorbed semivolatile organic compounds. The present effort is seen as a continuation of gathering and evaluating relevant atmospheric kinetic and thermodynamic data summarized in Crowley et al. [26] which is highly appreciated by the scientific community and helpful for many working in the field. The motivation for the study of the semivolatile organics was inspired by previous work on toluene and limonene [22, 27] on Kaolinite LO and ATD-C on the one hand, and on the other hand was influenced by the need to understand the interaction of partially oxidized organic semivolatiles thought to be important in secondary aerosol formation (SOA) in the presence of mineral dust within the troposphere. Here, the propensity of the adsorbate to undergo thermal and photochemical reactions is an important consideration even though it was not the primary focus of the present work. [27, 28] Although the choice of the molecular systems seems in part repetitive in view of past studies, it seemed important to screen several semivolatile organic compounds using a flowing gas technique that enables the measurement of molecular kinetic parameters such as the rate constants for adsorption (k_a, k_0) and desorption (k_d), as well as the absolute number of molecules taken up per cm^2 of a given mass of exposed mineral dust material at a certain partial pressure and gas residence time τ_s. We chose a flowing gas experiment across a Knudsen flow Reactor (KFR) using molecular beam sampling coupled to phase-sensitive detection. We insist on this latter point when using mass spectrometric detection in distinct contrast to residual gas MS detection practiced for instance by Usher et al. (2003) when using “sticky” gases whose surface residence times ($\tau_s = 1/k_d$) on surfaces of the vacuum system (Pyrex glass, stainless steel, Silicon rubber, etc…) is a multiple of the gas residence time of the gas ($\tau_g = 1/k_e$) where k_e is the measured rate constant for effusion of the gas out of the KFR. This feature is of particular importance when dealing with semivolatile organics that usually are “sticky” by virtue of their functional groups. Unreliable results are obtained when using residual gas analysis that depend on the level of the semivolatile background in the detection chamber. [29]

2. Experimental Method and Materials

We are limiting ourselves to a brief description of the used experimental method in view of the recent publication of a comprehensive review on the use of the Knudsen Flow Reactor (KFR) and its application to obtaining kinetic parameters in heterogeneous gas-substrate or multiphase chemistry

systems. [29] It is a flowing gas experiment equipped with phase-sensitive detection of an effusive (thermal) molecular beam formed at the exit orifice of the reactor and coupled to electron-impact quadrupole mass spectrometry where the signals are proportional to the flow out of the KFR. It is configured as a two-chamber flow reactor whose lower small-volume sample compartment (SC) contains the solid mineral dust sample itself located in a sample cup of 10.6 cm^2 surface area or a container of smaller dimension depending on the application. By actuating a plunger the leak-tight cover plate is lifted and exposes the sample to the gas flow admitted to the KFR. Its dimensions, exit orifices, collision frequencies and first-order gas effusion rate constants are given in Table 1. Moreover, the essential construction elements of the used KFR are displayed in Figure S1 (see Supporting Information). The relationship between flow F^i (molecule s^{-1}) and concentration [M] (molecule cm^{-3}) or pressure P_M (P_M = [M]/RT) within the KFR of volume V (cm^3) with k_e being the measured rate constant of molecular effusion out of the KFR) may be calculated as follows (equation (1):

$$F^i = k_e [M] V \quad (1)$$

Apart from the MS signals itself the most important parameter to be measured is the flow rate F^i into the KFR as it puts the relative MS signals on an absolute basis and enables the evaluation of loss rates owing to uptake or reaction of the probe gas on the solid substrate and/or desorption rates of adsorbates at a given temperature. The experimenter may choose one configuration out of 8, namely sample exposed/not exposed as well as four exit orifices of nominal 1 ,4, 8 and 14 mm diameter.

Figure 1 (top panel) displays a typical uptake protocol (uptake phase) followed by the desorption phase (lower panel) after saturation of the substrate. In this work the uptake experiments have all been performed using the (nominal) 1 mm Ø exit orifice whereas the desorption rates have been measured at different exit orifice diameters choosing among four possibilities displayed in Table 1. Specifically, the uptake phase of applinate at a flow rate of F^i = 3.1 10^{15} molecule s^{-1} starts with establishing a stable lock-in signal level at 1.7 V followed by opening the leak-tight sample compartment at 9500 pts (4 points recorded in one second). In response to the exposure of Kaolinite LO by lifting the plunger a rapid decline of the MS signal of applinate reveals a large loss rate owing to adsorption onto the solid substrate. The rapid loss of MS signal is followed by a gradual recovery indicating increasing saturation of the adsorption that is complete at approximately 14'300 pts. when the SC is closed again. Essentially no change in MS signal is observed which indicates complete saturation. In general several tests are undertaken after complete saturation of the solid sample but are not discussed n detail here. The loss rate integrated over time results in the total number of molecules lost to the sample interface. This integral corresponds to the difference in area between the inlet MS signal before the start of the uptake interpolated to the signal at total saturation resulting in a straight line and the actual recorded signal. In the case of Figure 1 (uptake phase) we have lost roughly 50% or more of the exposed molecules within the rectangle of 1.7 V or 3.1 10^{15} molecule s^{-1} times (14'300-9'500)/4 = 1200 s resulting in 1.9 10^{18} molecules lost. The actual number may be found in Appendix A1 and is smaller than the one based on a rough estimation above.

The desorption phase of a completely saturated sample is displayed in the lower panel of Figure 1 after halting the flow of applinate at approximately 22'000 pts. which is complete after the return of the MS signal to the baseline at approximately 27'000 pts. Owing to the "sticky" nature of applinate and the other semivolatiles used in this study it always takes some time to pump the rather large internal surface of the plenum of the KFR, on the order of 20 minutes or so. At approximately 28'000 pts. The plunger is lifted at once and an intense peak is observed decaying with time. This is the desorption rate of adsorbed applinate as a function of time and is of a complex non-exponential form to be discussed below. Before all molecules are desorbed in the 1mm Ø orifice reactor, that is before

the MS signal level has returned to the baseline, the 4, 8 and 14 mm Ø orifices are subsequently switched *in situ* giving rise to the remaining three peaks at approximately 33'000, 38'000 and 40'500 pts., respectively. In this way we are collecting all desorbing molecules in order to establish a mass balance between molecules adsorbed and desorbed. At the highest pumping rate corresponding to the 14 mm Ø orifice KFR the MS signal is close to the baseline and reassures us that we have pumped and recorded all available molecules during desorption. The desorption rates as a function of time will be evaluated below using a simple chemical-kinetic scheme depending on three rate constants.

The initial rate constant for adsorption (k_0) may be measured from uptake curves such as shown in Figure 1, upper panel under assumption of a first-order rate law commensurate with Langmuir adsorption, which states that the rate of adsorption is proportional to the number of free sites for adsorption. It is given by equation (2) with I_0 and I being the MS signals before and right after opening the SC and k_e the escape rat constant for a particular probe gas (see Table 1 for values):

$$k_0 = ((I_0 - I)/I)\, k_e \qquad (2)$$

If preferred, the initial uptake rate constants may be expressed in a dimensionless format as uptake probabilities corresponding to the fractional probability of being lost to the interface on the time scale of the experiment given by k_e. It may be expressed in equation (3) as follows:

$$\gamma_0 = k_0/\omega = ((I_0 - I)/I)\, (A_h/A_s) \qquad (3)$$

with ω the collision frequency (see Table 1), A_h and A_s being the areas of the escape orifice and the geometric sample surface, respectively.

Table S2 (see Supporting Information) reveals the identity and some pertinent data for the seven semivolatile probe gases used in this study, namely applinate, menthol, pipol acetate, limonene, γ-terpinene, toluene and benzylacetate and were all commercially available and of standard purity. The corresponding structural formulas are given in Scheme I. All samples were subjected to two cycles of freeze-pump-thaw before preparing samples in 2 or 5 l Pyrex glass bulbs except for menthol and benzylacetate that were used without a buffer volume given their small ambient temperature vapor pressure. Both Kaolinite LO (Low Order or "disordered") and ATD-C (Arizona Test Dust – Coarse) were commercially available samples with a BET surface area of 22.5 and 10.8 m^2/g measured using a Micromeritics automatic instrument. Specifically, Kaolinite LO, poorly ordered, was purchased from Source Clay Minerals Repository, University of Missouri-Columbia, 101 Geological Sciences Building, Columbia MO 65211 USA as KGa-2, provenance from Warren County, Georgia, USA, Arizona Test Dust Coarse (ATD 12103-1, A4) was purchased from Powder Technology Inc., 1433 Ewing Avenue S. Burnsville, Post Office Box 1464, MN 55306.

3. Results

3.1 Uptake of semivolatile organics on mineral dust

The semivolatile gas probes have been selected in terms of their functional groups. Applinate, a weakly oxidized organic compound is an ester of ethanol with 2-methylpentanoic acid (or 2-methylvalerate) and has two oxygen atoms whereas pipol is an ester of an unsaturated alcohol with acetic acid and also has two oxygen atoms and an unsaturated site on the alcohol side. Menthol has a hydroxyl group within a saturated terpene frame. Benzylacetate is an ester of acetic acid with benzylalcohol and has two oxygen atoms and an aromatic phenyl group whereas toluene has only a phenyl group. In view of the potential importance of atmospheric water vapor on adsorption/desorption kinetics we have included H_2O as a probe gas in the present study. Table 2

displays a synopsis of the most important data on uptake of the semivolatile probe gases on both mineral dust materials Kaolinite LO and ATD-C performed at ambient temperature. The fourth column from the left displays the monolayer saturation in % that uses an estimate for the absolute number of molecules making up a monolayer over 1 cm^2 of surface. Numerical values for this calculation for the seven used probe gases may be found in Table S2. Absolute numbers for the uptake of probe gases may be found in the fifth column of Table S1 (Supporting Information). The fifth column of Table 2 ("prompt desorption at saturation") expresses the number of desorbing molecules after total saturation of the interface in % of the number of adsorbed molecules measured in the uptake phase displayed in Figure 1a as an example. In order to determine the amount of adsorbed molecules desorbing over a longer time scale we pumped the sample overnight at the highest pumping rate (14 mm Ø KFR) and readsorbed the same sample with the probe gas the next morning. These values are displayed in the sixth column in % of the initially adsorbed amount at saturation. The seventh column lists the fraction of probe molecules persisting even after overnight pumping where the sum of percentages of column six and seven add up to 100%. Finally, column 8 of Table 2 displays the fraction of probe gas molecules pumped off overnight that is computed according to footnote a in Table 2 and algebraically corresponds to the difference between column 6 minus column 5.

As explained above the uptake is the integral over time of the loss rate of a particular semivolatile, that is the total absolute uptake in molecules on the exposed surface area of the substrate. Absolute numbers of semivolatile organics taken up may be found in the fifth column from the left margin of Table S1 (Supporting Information). The sixth column of Table S1 displays the fractional value per cm^2 of total internal and external (BET) surface in terms of a fractional monolayer adsorbed in order to enable quantitative comparisons between both mineral dust materials. Using a rough approximation for the number of molecules constituting a molecular monolayer displayed in Table S2 we have listed the fraction of adsorbed molecular monolayers in the fourth column of Table 2 as explained above. We take note of a large variability of fractional monolayer coverage going from 5 and 10% for menthol/Kaolinite and applinate/Kaolinite, respectively, to essentially 100% for pipol/ATD-C. For the latter case the actual number is larger than 100% and listed as a number in small font which has to do with the fact that no reliable quantitative determinations on saturation coverages exist in the literature. The coverages listed in Table S2 in terms of molecular monolayers should correspond to upper limiting values based on liquid densities that should correspond to lower limits of coverage. However, in the absence of the detailed geometric arrangement and surface-filling mode of the adsorbate we limit ourselves to the statement of "large" coverage in the above case that may be inaccurate up to a factor of 30%. However, it is a remarkable fact that to the exception of limonene and γ-terpinene all other semivolatile organics attain larger coverages on ATD-C compared to Kaolinite LO mineral dust materials. Turning to column 5 of Table 2 ("prompt" desorption) we find that the extent of desorption at ambient temperature in % of initial adsorption, occurring spontaneously after reaching saturation upon opening the sample compartment (SC) as displayed in Figures 1 and 2, is larger for Kaolinite LO than for ATD-C without exception. The semivolatile adsorbate limonene and γ-terpinene show no or small amounts of desorption. Apart from these latter two cases this trend is remarkable and qualitatively suggests that the bonding of the semivolatile is weaker on Kaolinite LO than on the ATD-C substrate. Visual comparison of the four desorption peaks in the upper and lower panel of Figure 2 confirms this conclusion in that the desorption peak areas for menthol/Kaolinite LO (upper panel of Figure 2) are significantly larger than for menthol/ATD-C (lower panel of Figure 2).

Once we run out of MS signal at the fastest pumping rate corresponding to the lowest gas residence time using the largest reactor orifice (14 mm Ø) in place for the observation of spontaneous

desorption as shown at t = 60'000 (upper panel in Figure 2) and 56'000 pts. (lower panel in Figure 2) does not mean that desorption has come to a halt altogether. Running out of MS signal merely means that the MS signal intensity is drowned in the noise of the lock-in amplifier signal. We have therefore continued to pump the exposed mineral dust sample overnight, usually for 14 to 18 hours using the largest reactor orifice, thus the fastest pumping rate, and performed a readsorption uptake the following day up to saturation similar to the initial uptake. These data are displayed in column 6 of Table 2 and are clearly marked as "Readsorption" experiments in Table S1 (second column). Except for benzylacetate the conclusion is identical to the results obtained in the "prompt desorption" experiments: during overnight pumping, desorption is faster for the physisorbed adsorbate on Kaolinite LO compared to ATD-C. Despite the heterogeneity of the binding sites encountered in surface science [30-32] the conclusions are robust when comparing the bond-strength between semivolatile organics interacting with Kaolinite LO and ATD-C. Despite the energetic spectrum of binding sites present on solid substrates often confirmed in thermal desorption experiments we are able to assert a larger affinity for bonding of semivolatiles in ATD-C compared to Kaolinite LO. Benzylacetate seems to be an exception, however, it may mean that the uncertainty of the adsorption/readsorption experiments is larger than 5% which would disable the comparison between 14.5 and 10.1 % displayed in Table 2. We are therefore unable to state on the bonding preference of benzylacetate for the interface of either Kaolinite LO or ATD-C.

Finally, we have performed a set of preliminary experiments in which a constant inflow of H_2O vapor was simultaneously met with a constant flow of applinate after saturation of both Kaolinite LO and ATD-C with water vapor. The concurrent flow of H_2O vapor and probe gas guarantees a constant coverage of H_2O once the probe gas has been admitted. It is of note that the inverse uptake experiment has not yet been performed in which an applinate-saturated mineral dust substrate is being exposed to water vapor as a function of time. Comparing sample runs FS10 with S243 and S244 (see Table S1) we observe an increase of the coverage at saturation of 30% and a factor of three, respectively, for applinate adsorption on Kaolinite LO. For an ATD-C substrate the applinate coverage increased by 20% comparing FS40 with S245 (see Table S1) under simultaneous inflows of H_2O and applinate at prior saturation coverage of H_2O vapor before admitting applinate. In summary the present preliminary experiments with concurrent H_2O/probe gas flows seem to indicate a modest increase in applinate coverage on H_2O-saturated Kaolinite LO and ATD-C substrates.

3.2 Kinetic Data: Desorption rates of semivolatile organics adsorbed on mineral dust – Surface residence times of semivolatiles

In order to extract chemical-kinetic rate constants from desorption (and adsorption) experiments we must first find a numerical or analytical solution to the integration of the rate law applicable to the particular experimental situation because the desorption rates as a function of time displayed in Figure 2 are non-exponential decays. Semilog plots of these experimental decays are strongly non-linear and do not correspond to an elementary rate constant. Scheme II below displays the different kinetic processes for the present KFR situation as follows: The green arrow represents the constant influx of gas in terms of F^i/molecule s^{-1} and is zero for a desorption experiment with previous saturation of the uptake of the semivolatile probe gas. The blue and red arrows represent the elementary process of adsorption (k_a) and desorption (k_d) of the probe gas, and the orange arrow corresponds to effusive loss of probe gas across the exit orifice of the KFR (k_e). The rate of uptake is the difference between the adsorption and desorption rate, and the values of k_e for any of the four exit orifices of the KFR are listed in Table 1 and correspond to measurements using "non-sticky" calibration gases (Iannarelli et al., 2022).

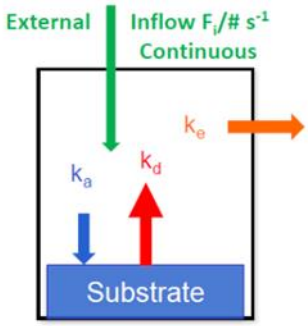

Scheme II

The rate law for the kinetic situation displayed in Scheme II is given in equation (4) wherein the first, second and third term on the right side of equation (4) correspond to desorption, adsorption and escape of probe gas for a saturated interface without constant influx of probe gas, that is with $F^i = 0$. This situation corresponds to desorption of a **saturated** interface as presented in Figures 2 and 3.

$$dN(t)/dt = k_d\, N_{max} \exp(-k_d t) - k_a\, N\, N_{max}\, (1 - \exp(-k_d t)) - k_e N\, (+ F^i) \qquad (4)$$

The symbols in equation (4) have the following meaning besides the rate constants discussed above: N(t) is the total number of probe gas molecules throughout the KFR at time t, and N_{max} is the total number of adsorbed semivolatile probe gas adsorbed at the interface of the solid mineral dust sample at saturation of adsorption. This simple rate-law is based on Langmuir adsorption whose adsorption rate is simply proportional to the amount of free surface adsorption sites. It naturally represents an approximation to the true more complex interface at hand. As a reminder, the simple Langmuir kinetic model assumes that (i) the surface is homogeneous, (ii) every adsorbed species occupies identical sites to every other species at all coverages, (iii) there are no (lateral or steric) interactions between adsorbed species, other than preclusion of occupation of a site by more than one adsorbed species, and (iv) there is no mechanism for the transport of impinging gas molecules across the surface by surface diffusion processes, for instance. The rate law (equation (4)) may be integrated in closed form as a function of time using the simple Langmuir kinetic model implicit in the rate law, equation (4) and results in equation (5) after integration as a function of time whether or not a constant inflow (F^i) is maintained.

$$\frac{N(t)}{N_{max}} = \frac{k_d\, e^{-k_d t}}{k_e - k_d + k_a(1 - e^{-k_d t})} - \frac{k_d}{k_e - k_d} \cdot e^{-((k_e + k_a)t - \frac{k_a}{k_d}(1 - e^{-k_d t}))} + \frac{F^i / N_{max}}{k_e + k_a\,(1 - e^{-k_d t})} \qquad (5)$$

Although complex, equation (5) only depends on three rate constants, namely the ones displayed in Scheme II when a desorption process occurs without external flow ($F^i = 0$ in equation (5)). It also is apparent that it is not a single exponential as a function of time. The simplest case is realized when k_e and k_a are known from calibration (Table 1) and from the uptake phase, respectively, when k_a equals k_0, the measured heterogeneous uptake rate constant in the uptake phase, that is on a virgin substrate. In that case $N(t)/N_{max}$ as a function of time would theoretically just be a single parameter fit were it not for the scaling factor N_0/N_{max}. This additional scaling factor is necessary in practice because upon exposing the substrate the probe gas molecules also interact with the clean vessel walls of the sample compartment during the uptake phase and result in a short term burst of gas dominating the desorption experiment at short times. Once this relatively short burst of gas is over desorption originates exclusively from probe gas molecules adsorbed to the substrate. In practice the

effect of probe gas adsorption onto the clean vessel walls of the SC is experimentally measured in an uptake/desorption experiment performed in an empty SC without a substrate and is numerically taken into account by an additional scaling parameter. It is important to realize that k_0 addresses the virgin state of the interface devoid of any adsorbate prior to uptake, whereas k_a corresponds to interaction with the interface saturated with the semivolatile probe gas right after the beginning of the desorption phase opening the SC to the plenum of the KFR.

A look at obtained data displayed in Figures 3, 4 and 5 and summarized in Table 3 may be helpful at this point. Figures 3 and 4 display the desorption kinetics of applinate from a saturated substrate of Kaolinite LO and ATD-C, respectively, Figure 5a and 5b display benzylacetate desorption on both substrates. Invariably, the data show an initial desorbing burst of semivolatile material NOT coming from the substrate, but from the saturated walls of the SC as measured by the reference experiment using the empty SC devoid of any substrate mass and briefly mentioned above. The degree of this parasitic effect based on adsorption of probe gas to the vessel walls depends on structural and thermodynamic parameters of the probe gas. As an example wall adsorption of H_2O vapor is minimal, followed by toluene and applinate, where the effect is significant upon performing a reference experiment on an empty SC (R248, R249 displayed in Table S1). Between applinate and toluene there is a factor of 4.7 in terms of total molecules adsorbed at saturation in an empty SC and at ambient temperature. Throughout the probe gas series the adsorbed fraction on the SC vessel walls comprises between roughly 5 to 15% of the total that instantly desorbs upon lifting the plunger depending on the type of probe gas which may be seen in Figures 3 to 5 as the portion not taken into account by equation (5). Desorption of semivolatile gas from the substrate follows a longer rise and decay time traced in red. Columns 4 and 5 of Table 3 list the measured value of k_0 and k_a for all semivolatile probe gases including H_2O vapor interacting on both solid substrates except limonene and γ-terpinene with Figures 3, 4 and 5 providing visual support for two probe gases. Of note is the similarity between k_0 and k_a for applinate, pipol, menthol and benzylacetate/Kaolinite LO whereas benzylacetate/ATD-C as well as toluene on both substrates show a significant difference between k_0 and k_a. Depending on the bond strength and lifetime of the adsorbate k_a measured during the desorption phase (saturated state) and k_0 measured during uptake phase (virgin state) do not need to be equal because both types of experiments address a different state of the interface, saturated for desorption, and clean for the uptake experiment.

Table 3 displays the fitted parameter k_d which corresponds to a slow process of desorption that operates as a source term in contrast to k_a and k_e that work as a sink in equation (4). In most cases k_0, the rate constant for uptake of probe gas on a virgin substrate is quite similar to k_a, the fitted rate constant for adsorption in the desorption case at saturation of the probe gas. However, for toluene interacting on both substrates and benzylacetate/ATD-C we find $k_a > k_0$. Also, in the latter case k_d seems significantly larger than for the former cases of near equality between k_0 and k_a. There seems to be a smooth transition during saturation between the beginning of the uptake (k_0) and the end close to saturation (k_a), and vice-versa for returning from saturation towards the desorbed state of the interface during a desorption measurement. In order to capture the transition from k_a to k_0 for desorption we have used the following empirical interpolation formula wherein the time scale is given by the fitted k_d parameter, equation (6):

$$k_a(t) = k_0 \left(1 - \exp^{-k_d t}\right) + k_a \exp^{-k_d t} \tag{6}$$

Knowing full well that application of equation (6) represents an empirical (assumed) relationship we draw attention to Figure 5a and b dealing with benzylacetate on both mineral dust materials resulting in an acceptable fit in both cases with k_d listed in Table 3. Implementing a significant change

of k_a during the adsorption and desorption phase would have complicated the search for a closed solution of the three parameter model displayed in Scheme II and equation (5). We also want to point out that between limonene and γ-terpinene only the latter desorbs from ATD-C, in the three other cases no desorption signal clearly attributable to desorption from the sample had been obtained.

The surface residence time $1/k_d$ in seconds is listed in column seven of Table 3 and shows a fairly large variation, both between the two mineral dust materials and between the different semivolatile probe gases. Generally, $k_d << k_a$ at ambient temperature such that the measured uptake is numerically equal to k_a, the elementary rate constant for adsorption leading to equality between uptake and mass accommodation for the present series of probe gases at ambient temperature.

3.3 Kinetic Data: Adsorption rates of semivolatile organics on mineral dust interface

The last part of our kinetic investigation deals with the measurement of the initial uptake coefficient γ_0 where "uptake" here means the elementary process of adsorption given that spontaneous desorption (k_d) is orders of magnitude slower than k_a such that there is no interference in the process of molecular adsorption of the semivolatile probe gas. The results are displayed in Table 4 following an experimental protocol exhibited in Figures 6 and 7. The chemical kinetics presented in this section refers to the files S224 to S227, S230 to S235 and S237 listed in Table S1. Owing to the fact that the γ_0 values were close to unity we chose to use sample cups of smaller diameter corresponding to 0.29 and 1.131 cm^2 (Table 4). We started to expose the mineral dust sample at a constant flow rate into the KFR and the lowest partial pressure, that is in the 14 mm Ø orifice, in order to avoid as much as possible saturation of the interface during initial uptake. After a short uptake period we closed the SC, changed to the next higher partial pressure at constant flow rate (8mm Ø orifice) and opened the SC to the flow of the probe gas. This process was repeated for the 4 and 1 mm Ø orifice all the while minimizing the exposure duration of the sample to the probe gas (see Figure 7). At the end of this measurement series we came back to the 14 mm Ø orifice where we started from in order to gauge the reduction in γ_0 owing to saturation during the measurement of the initial uptake coefficient. These smaller values for the 14 mm Ø orifice are given in Table 4 in small print below the initial value in bold (column 6 of Table 4). The downward spikes of the MS signal upon changing the aperture stems from the filling transient when going from low to a higher partial pressure, say from 14 to 8 mm Ø orifice at 5'700 pts. in Figure 6 or 9'700 pts. in Figure 7 because the orifice changing mechanism always goes via briefly emptying the KFR at high pumping rate. When the intended orifice is in place the KFR has to be refilled until steady-state is reached. This becomes especially apparent when changing from the 4 to 1 mm Ø orifice KFR because the time scale for filling the KFR to a steady state value is tens of seconds owing to the small value of k_e. This may be observed at 11'300 pts. in Figure 7 for γ-terpinene/Kaolinite LO. However, the filling effect is absent when opening the SC and performing the kinetic uptake measurement owing to the small volume of the SC compared to the plenum of the KFR (50 vs. 1830 cm^3). Moreover, there is a decrease in steady-state MS intensity when changing the exit orifice at constant flow rate. The expectation is one of constant MS signal level, however, owing to small misalignment and other geometric factors there is a noticeable decrease in MS signal intensity with decreasing exit orifice Ø, especially when going from the 14 to 8 mm Ø orifice.

There are two types of uptake kinetic traces exemplified in Figure 6 and 7. In Figure 6 with limonene being the only member of the semivolatile set that shows this behavior, the MS signal remains at a constant level except for the first uptake in the 14 mm Ø orifice which shows a brief "glitch", but only

for the first exposure. The constant, that is non-saturating MS signal level means that limonene undergoes a chemical reaction whose reaction product either evaporates or does not impede further adsorption of semivolatile probe gas. The second type is exemplified in Figure 7 and includes the six remaining semivolatiles which show a distinct saturation behavior, even after the maiden opening of the SC in the 14 mm Ø orifice KFR. A telling experiment is sample S237 displayed in Table 4 where two repetitions of SC openings already lowered γ_0 from 0.36 to 0.32. After performing the full set of experiments using the 8, 4 and 1 mm Ø orifice saturation has progressed such that the third uptake at the end coming back to the 14 mm Ø orifice resulted in $\gamma_0 = 0.11$, a factor of three smaller than the initial uptake which suggests rapid saturation of the substrate interface.

We recommend the "maiden experiment" performed in the 14 mm Ø orifice KFR and listed in bold characters in Table 4 as every subsequent experiment gradually resulted in smaller values owing to saturation of uptake. Generally, we note the large values for γ_0 except for toluene on both types of mineral dust materials ranging from 0.3 to 0.8. Values in excess of $\gamma_0 = 0.5$ have large inherent uncertainties of ± 25%. Table 4 reveals a crowded field of γ_0 with all semivolatiles except toluene as far as the magnitude of γ_0 is concerned. For toluene γ_0 is twice as large for the interaction with ATD-C compared to Kaolinite LO. At the end we emphasize that for initial values of the uptake coefficient as opposed to its steady-state value (if there is one) the geometric surface is the only one justifiable from the gas-kinetic point of view irrespective of sample mass used in essence because of the time it takes to probe the subsurface structure of the powder mass.

3.4 Uncertainties: systematic and random (statistical) errors

Working with semivolatile probe gases is demanding in terms of temporal resources of the experimenter: the length of data acquisition files sometimes extends from 50'000 to 70'000 data points at a recording frequency of 4 s^{-1} corresponding to several hours that a combined uptake/desorption experiment may take. Apart from a few duplicate experiments (see Table S1) we have decided to concentrate on the survey aspect of the present work and its systematic nature encompassing seven semivolatile gases and two commonly used mineral dust materials. This also means that we are unable to state statistical random measurement errors for each uptake or kinetic measurement as systematic uncertainties dominate the present measurements. However, we will in what follows estimate some of the weak points of the experiments and derive a realistic measure of uncertainty of the experimental results obtained.

Uptake measurements which represent the bulk of the reported results have been performed on a modest amount of sample mass spread out over a sample cup of 10.6 cm^2. Too large a sample mass would have needlessly prolonged the uptake measurements, and would also imply the disadvantage that we would have measured a rate constant for adsorption (k_0) that does not correspond to one coherent layer of sample exposed to the probe gas, but less than a single layer. Therefore, we are unable to measure the initial uptake coefficient γ_0 from these experiments. On the other hand, by choosing a small mass we minimize the mass transfer of probe gas adsorbed to the interface into the bulk sample such that we obtain a saturation coverage of the interface mainly at the expense of bulk adsorption. Table S1 displays (quasi-)steady-state rate constants for mass transfer into the bulk that are roughly 100 to 1000 times smaller than k_0 so that we conclude that we "loose" 1% or less of the probe molecules to the bulk. The higher the bulk mass with respect to the interface, the more important is the loss to the bulk that has to be quantified using a theory of diffusion of a gas into a solid heap of powder [33] because bulk diffusion and adsorption to the interface become increasingly competitive as we have shown in the example of the interaction of HNO_3 on salt [34]. We conclude that

we have a systematic uncertainty of roughly 1% in k_0. In addition, we increase this number by a factor of ten for (a) a sloping MS signal during the uptake owing to a small change of vapor pressure of the semivolatile during the measurement, and (b) a measurable change of the inlet flow rate at the beginning and the end of the uptake experiment, for whatever reason. In the end we use the different time scales of the experiment to distinguish unequivocally between interface and bulk adsorption in the aftermath of mass transfer into the bulk.

However, by far the largest uncertainty in monolayer coverage comes from the estimate of the number of molecules making up a monolayer coverage on the substrates of interest. These numbers listed in Table S2 are rough estimates based on the density of the liquid phase and are uncertain by a factor of two, in both directions. Furthermore, it is improbable that both mineral dust substrates used in this study would have a common interface coverage owing to their different nature and structure of the interface. However, using this simple volumetric model is the best we can do at this time of missing interfacial information on the properties of solid mineral dust materials.

The requirements of the kinetic (Table 4) are different from the uptake (Table 2) experiments in that a coherent layer of mineral dust material has been used on a smaller geometric surface area in order to enable the measurement of γ_0 and be certain that at least a coherent layer of material was present for the measurement. Owing to the large values of γ_0 we had to lower the geometric surface when using the 1 mm Ø KFR in order to fall within the 50 ± 10% decrease of the MS signal upon uptake which affords the highest precision when using equation (3). Figure 1 (applinate/Kaolinite LO) shows a case in point for the 1 mm Ø KFR where the MS signal practically drops to zero after opening the SC thus making a meaningful measurement of γ_0 impossible. Owing to the small mass transfer into the bulk and the short observation period for the kinetic measurement we do not incur an uncertainty larger than 10% unless the uptake probabilities tend towards unity. At this point small uncertainties in the gas-surface collision frequency ω lead to large uncertainties in γ_0 as shown in Table 4. We chose the 14 mm Ø KFR for the measurement of γ_0 because it is the least probable to be influenced by saturation and the most accurate to measure owing to the low extent of MS signal decrease.

There are a few examples where essentially the same uptake experiment has been performed as a set of multiples in order to obtain an idea about the uncertainty in coverage of the probe gas benzylacetate interacting with ATD-C (see Table S1). Comparing experiments S203, S236 and S238 we obtain coverages of 18.4, 15.4 and 19.1%, respectively, which agree to within less than 5% of a monolayer. However, the recovery of the probe gas by spontaneous desorption amounts to 23.6, 7.8 and 31.6 % of the number of molecules taken up which may be due to different lengths of pumping the solid substrate ATD-C before uptake, a problem recognized especially with ATD-C compared to Kaolinite LO. However, a caveat should be placed on the comparison of S209 with S224 corresponding to limonene interacting with Kaolinite LO. Both data sets are not comparable owing to the fact that the former has been obtained in the 1 mm Ø orifice KFR whereas in the latter experiment the 14 mm Ø KFR has been used. The coverage is higher by a factor of 5 in the 1 compared to the 14 mm Ø KFR owing to a factor of 130 in partial pressure of limonene at comparable flow rates into the KFR. It is useful to remember that saturation coverages are determined at the highest partial pressure whereas the opposite is true for the measurement of the initial uptake rate constant (k_0) or probability (γ_0). Two other sets of experiments lend themselves to direct comparison: H_2O/Kaolinite of experiments S243 and S244 leading to a saturation coverage of 7.8 and 7.7% of a monolayer, respectively (Table S1). Another set is H_2O/ATD obtained in experiments S245, S246 and S247 (Table S1) leading to a saturation coverage of 22.1, 20.1 and 22.1 % of a molecular monolayer. Spontaneous desorption in experiments A246 and S247 led to a recovery of 79.0 and 70.0% of the

saturation coverage. We may therefore state that the reproducibility is within 15% in favorable cases.

We therefore have the situation that the present measurements offer a reasonable, that is fairly low, uncertainty as far as the determination of absolute numbers of molecules taken up (Table S1, fifth column from the left) are concerned, but face a large uncertainty, say a factor of two or so, in "reduced" albeit convenient quantities such as coverages in molecular monolayers.

4. Discussion

As alluded to in the Introduction to this study, similar studies on the physisorption and reaction with or without sunlight of organic semivolatiles in the presence of mineral dust materials are sparse. In a study of gaseous limonene with Kaolinite, ATD, silica (SiO_2) and γ-Al_2O_3 Lederer et al. (2016) observed a chemical oxidation reaction to limonene oxide, an epoxide of the endocyclic double bond, via oxidation or atomic oxygen transfer to limonene at the interface of mineral dust materials that subsequently hydrolyzed to the vicinal 1, 2-limonene diol. [27] Secondary reactions of this diol yielded additional oxygen-containing products such as carvone and carveol. Prior exposure of mineral dust materials to HNO_3 accelerated/enhanced this redox reaction. In addition, acid or base-catalyzed surface sites will lead to hydration products of adsorbed limonene, such as terpineol. [35] There is an apparent link of the present redox and hydration reactions to the catalysis literature for the specific case of limonene [36], but also for both gaseous and liquid catalytic terpene conversion in general in special consideration of natural and synthetic zeolites and clay minerals. [37, 38] The only semivolatile organic compound undergoing strong physisorption or even chemisorption under our conditions is limonene because (a) no desorption was ever observed on either of the investigated mineral dust materials, (b) no gas-phase reaction product became apparent in the course of the adsorption/desorption experiments, and (c) no apparent saturation of the interface could be observed (Figure 6) in comparison with all other semivolatiles investigated. Concerning point (c) it must be noticed that limonene saturated at 10 and 41% of a monolayer on ATD-C and Kaolinite LO, respectively, in comparison to the geometric isomer γ-terpinene that saturated at 7.5 and 12% on ATD-C and Kaolinite LO, respectively. This explains in part the increased propensity towards saturation of γ-terpinene compared to limonene on both mineral dust substrates. An additional strong argument for chemisorption or reaction of limonene on both mineral dust materials comes from the fact that it is the only semivolatile probe gas investigated that showed any steady-state uptake after (partial) saturation as shown in the last column of Table S1. The steady-state rate constants for limonene are an order of magnitude higher than for γ-terpinene and other semivolatile probe gases where this slow process has been generally interpreted as a mass transfer diffusion process or equivalent first-order rate constant for the diffusion of probe gas initially adsorbed to the interface deeper into the bulk part of the sample. [39] However, long-term observation of this "steady-state" mass transfer phenomenon reveals that the magnitude slowly decreases with time concomitant with the increasing saturation of the bulk phase of the sample. Therefore, we may preferably speak about a "quasi-steady-state" phenomenon.

In any case we would not expect to observe the limonene epoxide under our conditions, a precursor to the observed 1,2-vicinal diol in the atmosphere, because of the absence of O_2 in the KFR. It has been established that both catalytic and environmental redox reactions only occur in the presence of O_2 which is the oxidizer, the interface merely contributes the catalyst to turn the reduced organic matter into a weakly or highly oxidized organic compound using air oxygen as the primary oxidizer, both in the gas- as well as in liquid phase. [39] We therefore believe that adsorption of limonene to the

interface of both mineral dust materials generates a strongly bound precursor within the KFR that could undergo oxidation in the presence of air oxygen once the KFR is vented to atmospheric conditions. In the case of γ-terpinene the situation may be similar except that limonene adsorbs 3.5 times more to saturation than γ-terpinene (40.8 vs. 12.2 % of a molecular monolayer for limonene and γ-terpinene, respectively. See Table 2).

Another study remotely related to the present investigation deals with a laboratory investigation of the interfacial reaction of the oxidizer NO_2 with toluene in the presence of mineral dust materials with and without UV radiation (SiO_2, α-Fe_2O_3, Fe(II)- and Fe(III)-sulfate minerals) by Niu et al. [28] As expected, various oxidation products of toluene such as o-nitrotoluene and benzaldehyde were detected by *in situ* DRIFTS IR spectroscopy at different experimental conditions, however, the observables do not support the conclusions with respect to the mechanism of the heterogeneous reactions. In another study similar to the present approach Chen et al. [40] have studied the interaction of humic acid (HA) on Kaolinite using dynamic ATR-FTIR combined with XPS in an effort to put the adsorption on a molecular basis as a function of pH of the aqueous slurry thus perhaps affecting the surface functional groups of both HA and Kaolinite. This seems nevertheless to be a promising approach, but is hampered by the fact that both components of the interaction pair (HA/Kaolinite) are complex implying unknown consequences of interface composition of both components upon perturbation.

Moreover, an excellent report on the nitration of the polycyclic aromatic hydrocarbon pyrene highlights the efficient reaction in the presence of Chinese Desert Dust (CDD), clay minerals (Kaolinite, Montmorillonite) and ATD using the heterogeneous nitration of pyrene to 1-nitropyrene as a quantitative gauge of the efficiency of the nitration reaction [41]. The detailed heterogeneous reaction mechanism essentially remains unknown, however, the consensus goes in the direction of the potential importance of some electrophilic species such as $N_2O_4H^+$, akin to electrophilic aromatic substitution of NO_2^+ as the active nitration species used in the chemical industry. In the past, excellent analytical work on nitration of polycyclic aromatic hydrocarbons adsorbed on carbonaceous as well as mineral dust materials has been performed by Esteve et al. [42, 43], Miet et al. [44] and topped by a flowing gas kinetic investigation by Nguyen et al. [45] For pyrene the exclusive product of nitration by gas phase NO_2 is 1-pyrene, a toxic and probably carcinogenic compound. [46] The surprise lies in the fact that complex interfaces such as Chinese Desert Dust (CDD), primarily made up of a heterogeneous mixture of quartz, corundum (α-Al_2O_3, clay minerals, carbonates, feldspars and hematite (α-Fe_2O_3) (in the order of decreasing importance of weight of the different contributors), undergo the heterogeneous nitration reaction of adsorbed pyrene at a much higher rate than the separate constituents themselves (see Table 1 of Kameda et al. [41]). In addition, on many of the components 1-nitropyrene further reacted to polynitropyrenes, once the supply of unsubstituted adsorbed pyrene was exhausted. In addition, using pyridine adsorption monitored using IR DRIFTS they showed that the nitration reaction is accelerated, especially on clay mineral substrates which underlines the necessity of providing acidic sites for efficient nitration. Many of the simple components of mineral dust by themselves, such as α-Al_2O_3, SiO_2, TiO_2, α-Fe_2O_3, feldspars, carbonates, sulfates, or most importantly, NH_3-deactivated ATD had observed rate constants smaller by up to three orders of magnitude compared to Chinese Desert Dust (CDD), montmorillonites or ATD. This fact complicates the investigations but throws us in the right direction compared to the long held view that the reactivity of mineral dust followed the mixing ratio of its components as in Usher et al. [2] This result also puts a question mark on the theoretical approach taken by Keshavarz et al. [23] who took ortho-silicic or trisilicic acid as a surrogate for mineral dust materials which is a truly questionable approach given the conclusions of Kameda et al. [41].

The important group of main messages that we have formulated in the next section resulting from our current work are for the moment unmatched in that these data are filling a critical gap in terms of variability of coverage, as uncertain it may be in terms of numerical accuracy. This holds both for the uptake, but also for the initial uptake and desorption kinetics (k_a, k_0, γ_0). The kinetic data k_a and k_d in Table 3 fall into two groups putting aside limonene and γ-terpinene that essentially do not desorb: the first group consists of applinate, pipol and menthol which are semivolatiles where k_a is approximately equal to k_0 ($k_a = k_0$) for both mineral dust materials. This situation effectively leads to a single parameter fit (k_d) excluding the scaling factor given in Table 3 and displayed as an example in Figure 3 (applinate/Kaolinite LO). The second group includes benzylacetate and toluene on both mineral dust samples that is characterized by the inequality $k_a > k_0$ to a variable extent depending on k_e. This leads to a two-parameter fit excluding the scaling factor where both variables k_d and k_a are freely varied under the constraint of minimum deviation from the data over a given time interval. As an example Figure 5 displays the fit for benzylacetate on both mineral dust materials with the relevant fitting parameters for both fits exhibited in Table 3. We have encountered a similar situation for the interaction of small polar molecules on Processed Amorphous Carbon [39] where trifluoroacetic acid, trimethylamine and thiophene belonged to the first group ($k_a = k_0$), and highly polar molecules such as H_2O, HCl and NO_2 to the second ($k_a > k_0$).

In analogy to the situation with PAC the first group of semivolatile organics seems to follow the Langmuir model for adsorption with the build-up of a smooth or coherent adlayer of semivolatile molecules on both mineral dust materials. The beginning of adsorption to a clean mineral dust interface is characterized by k_0, the kinetic rate constant controlling the initial uptake of the semivolatile. Desorption and adsorption in a KFR are processes depending on three rate processes that are occurring simultaneously. The fact that $k_a = k_0$ means that desorption is taking place with gradual increase of free adsorption sites. For the second group with $k_a > k_0$ the adsorption is taking place on already adsorbed molecules forming nanodroplets or molecular clusters at the interface, thereby increasing the rate constant for adsorption on already existing droplets or clusters rather than adsorption on sites on the mineral dust interface as these most likely run out for adsorption owing to saturation. It appears that the Langmuir concept of free surface sites does not hold in this instance owing to the fact that incoming organic probe molecules are associating themselves to already adsorbed probe molecules owing to a larger thermodynamic affinity with adsorbed probe gas than with surface sites. In addition, the values of k_d that we primarily sought are much larger compared to the first group when $k_a > k_d$ because the nature of the interface has changed. Few adsorbed droplets or molecular clusters distributed at the interface are now the preferred adsorption sites rather than adsorption sites on the substrate itself. Three parameters seem to suffice to describe the temporal decay of the adsorbate, however, the meaning of two of the parameters (k_a, k_d) will have to be reinterpreted if one wants to uphold Langmuir kinetics for these substrate/probe pairs. Finally, we have to concede that alternative techniques of investigating the composition of the interface of mineral dust exist as outlined in Chen et al. [40] that are less detailed as presented in this report and in which the emphasis is placed on other functional groups or changes thereof.

5. Conclusions

The present study performed at ambient temperature involves the heterogeneous chemical-kinetic interaction of seven semivolatile probe gases with different functional groups in part representing terpenes and weakly oxidized hydrocarbons with two often investigated mineral dust materials

Kaolinite LO and Arizona Test Dust Coarse (ATD). The uptake varied from 100% of a molecular monolayer for pipol acetate/ATD down to 3% for toluene/Kaolinite with H_2O vapor being at 20% for ATD. In general, the coverage of the semivolatile probe gases was higher on ATD than on Kaolinite. Limonene and γ-terpinene were the exception in that their coverage on Kaolinite was larger than on ATD. The higher affinity of the semivolatiles towards ATD rather than to Kaolinite was confirmed when the spontaneous desorption yield immediately following uptake and long-term pumping was considered. Limonene did not show any desorption owing to a presumed chemical reaction on both mineral dust materials, and γ-terpinene showed minimal desorption yields on both mineral substrates. Initial uptake coefficients γ_0 were in the range 0.25-0.80 except for toluene with γ_0 of 0.1 and 0.2 on Kaolinite and ATD, respectively. However, all semivolatile/ATD and Kaolinite interactions were prone to saturation except for limonene. Owing to small desorption rate constants γ_0 may be interpreted as an accommodation coefficient in all cases. Extraction of rate constants was performed using a simple Langmuir adsorption model that enabled an analytical solution to the desorption data as a function of time in terms of rate constants for effusion (k_e), adsorption (k_a) and desorption (k_d). Except for the terpenes the semivolatiles, namely applinate acetate, ethyl 2-methylvalerate (pipol), menthol and benzylacetate/Kaolinite followed simple Langmuir adsorption with a fractional monolayer limit to saturation whereas toluene and benzylacetate/ATD did not. It is thought that in this latter case adsorption is taking place at a few suitable sites on the mineral dust material with molecules adsorbing onto already adsorbed probe gas molecules thereby building up nanodroplets or molecular clusters rather than a smooth adlayer. The surface residence times ($1/k_d$) varied from 50 to 40'000 s for toluene/ATD to menthol/ATD with 3'000 s for H_2O vapor on both mineral substrates. No obvious physical or chemical parameter of the semivolatile probe gas could serve as a predictor for the adsorption or desorption behavior for heterogeneous interaction in the present study. Predictability in this regard will have to wait until a more complete data base will have been acquired.

Supporting Information

Table S1 presents a master list of all performed experiments in the framework of this study, Table S2 displays estimated values of molecular monolayers of the seven investigated semivolatile organics and Figure S1 schematically presents the essential design elements of the Knudsen flow reactor used.

Acknowledgements

The authors thank SSIE/ENAC/EPFL and CPM/LBK/ENE/PSI for laboratory and personal resources enabling the present systematic study entirely supported by internal funds.

Bibliographic References

(1) Andreae, M.O.; Rosenfeld, D. Aerosol-Clouds-Precipitation Interactions. Part I : The Nature and Sources of Cloud-Active Aerosols. *Earth-Sci. Rev*. **2008**, *89*, 13-41

(2) Usher, C.R.; Michel, A.E.; Grassian, V.H. Reactions on mineral dust. *Chem. Rev.* **2003**, *103*, 4883-4939; doi: 10.1021/cr020657y

(3) Tang, M.; Huang, X.; Lu, K.; Ge, M.; Li, Y.; Cheng, P.; Zhu, T.; Ding, A.; Zhang, Y., Gligorovsky, S. et al. Heterogeneous reactions of mineral dust aerosol: Implications for tropospheric oxidation capacity. *Atm. Chem. Phys.* **2017**, *17*, 11727-11777; doi.org/10.5194/acp-17-11727-2017

(4) IPCC 2021: 6th Assessment Report (AR6): https://www.ipcc.ch/report/sixth-assessment-report-working-group-i/https://www.ipcc.ch/report/sixth-assessment-report-working-group-i/

(5) Chen, G.; Canonaco, F.; Tobler, A. et al. European aerosol phenomenology – 8 : Harmonized source apportionment of organic aerosol using 22 Year-long ACSM/AMS datasets. *Env. International* **2022**, *166,* 107325; doi.org/10.1016/j.envint.2022.107325

(6) Carlton, A. G.; Wiedinmyer, C.; Kroll, J. H. A Review of Secondary Organic Aerosol (SOA) Formation from Isoprene. *Atmos. Chem. Phys*. **2009**, *9*, 4987–5005

(7) Seinfeld, J.H.; Pandis, S.N. Atmospheric Chemistry and Physics: From Air Pollution to Climate Change; John Wiley & Sons, **2016**

(8) Kanakidou, M.; Seinfeld, J.H.; Pandis, S.N.; Barnes, I.; Dentener, F.J.; Facchini, M.C.; Dingenen, R.V.; Ervens, B.; Nenes, A.N.; Nielsen, C.J. et al. Organic Aerosol and Global Climate Modelling: A Review. *Atmos. Chem. Phys*. **2005**, *5*, 053–1123

(9) Tu, P.; Johnston, M.V. Particle Size Dependence of Biogenic Secondary Organic Aerosol Molecular Composition. *Atmos. Chem. Phys*. **2017**, *17*, 7593–7603

(10) Li, P.; Perreau, K.A.; Covington, E., Song, C.H.; Carmichael, G.R.; Grassian, V.H. Heterogeneous reactions of volatile organic compounds on oxide particles of the most abundant crustal elements: Surface reactions of acetaldehyde, acetone and propionaldehyde on SiO_2, Al_2O_3, Fe_2O_3, TiO_2 and CaO. *J. Geophys. Res.* **2001**, *106(D4)*, 5517-5529; doi.org/10.1029/2000JD900573

(11) Carlos-Cuellar, S. ; Li, P.; Christensen, A.P.; Krueger, B.J.; Burrichter, C. ; Grassian, V.H. Heterogeneous Uptake Kinetics of Volatile Organic Compounds on Oxide Surfaces Using a Knudsen Cell Reactor: Adsorption of Acetic Acid, Formaldehyde and Methanol on α-Fe_2O_3, α-Al_2O_3 and SiO_2. *J. Phys. Chem. A* **2003**, *107*, 4250-4261; doi: 10.1021/jp026760 9

(12) Laidler, K.J., Chemical Kinetics, 3rd Edition, Harper & Collins Publishers, Inc., **1987**

(13) Israelachvili, J.N., Intermolecular and Surface Forces, Third Edition 2011, Academic Press, Elsevier; DOI: 10.1016/B978-0-12-375182-9.10001-6

(14) Wang, X.; Romanias, M.N.; Pei, Zh.; Rousseau, A. ; Thévenet, F. Uptake Mechanism of Acetic Acid onto Natural Gobi Dust. *ACS Earth Space Chem*. **2020**, *4*, 1650-1662; https://dx.doi.org/acsearthspacechem.0c00168

(15) Ibrahim, S.; Romanias, M.N.; Alleman, L.Y.; Zeineddine, M.N.; Angeli, G.K., Trikalitis, P.N.; Thévenet F. Water Interaction with Mineral Dust Aerosol: Particle Size and Hygroscopic Properties of Dust. *ACS Earth Space Chem.* **2018**, *2*, 376-386; DOI: 10.1021/acsearthspacechem.7b00152

(16) Bedjanian, Y.; Romanias, M.N.; El Zein, A. Interaction of OH free radicals with Arizona Test Dust. *Atmos. Chem. Phys*. **2013**, *13*, 6663-6686; https://doi.org/10.5194/acp-13-6663-2013

(17) Pradhan, M.; Kalberer, M.; Griffiths, P.T.; Braban, C.F.; Pope, F.D.; Cox, R.A.; Lambert, R.M. Uptake of gaseous hydrogen peroxide by submicrometer titanium dioxide aerosol as a function of relative humidity, *Environ. Sci. & Technol*. **2010**, *44*, 1360-1365

(18) Wang, W.G.; Ge, M.F.; Sun, Q. Heterogeneous uptake of hydrogen peroxide on mineral oxides, *Ch. J. Chem. Phys*. **2011**, *24*, 515-520

(19) Romanias, M.N.; El Zein, A.; Bedjanian, Y. Heterogeneous interaction of H_2O_2 with TiO_2 surface under dark and UV light irradiation conditions. *J. Phys. Chem. A* **2012**, *116*, 8191-8200

(20) Romanias, M.N.; El Zein, A.; Bedjanian, Y. Uptake of hydrogen peroxide on the surface of Al_2O_3 and Fe_2O_3. *Atmos. Environ*. **2013**, *77*, 1-8

(21) El Zein, A.; Romanias, M.N.; Bedjanian, Y. Heterogeneous interaction of H_2O_2 with Arizona Test Dust. *J. Phys. Chem*. A **2014**, *118*, 441-448;

(22) Romanias, M.N.; Ourrad, H.; Thévenet, F.; Riffault, V. Investigating the heterogeneous interaction of VOC's with natural Atmospheric Particles: Adsorption of Limonene and Toluene on Saharan mineral Dusts. *J. Phys. Chem. A* **2016**, *120*, 1197-1212; DOI: 10.1021/acs.jpca.5b10323

(23) Keshavarz, F.; Shcherbacheva, A.; Kubečka, J.; Vehkamäki, H.; Kurtén, Th. Computational Study of the Effect of Mineral Dust on Secondary Organic Aerosol Formation by Accretion Reactions of Closed-Shell Organic Compounds. *J. Phys. Chem. A* **2019**, *123*, 9008−9018; DOI: 10.1021/acs.jpca.9b06331

(24) Tong, H.; Lakey, P.S.J.; Arangio, A.M.; Socorro, J.; Kampf, C.J.; Berkemeier, T.; Brune, W.H.; Pöschl, U.; Shiraiwa, M. Reactive oxygen species formed in aqueous mixtures of secondary organic aerosols and mineral dust influencing cloud chemistry and public health in the Anthropocene. *Faraday Discuss*., **2017**, *200*, 251

(25) Xu, K.; Liu Y.; Li, C.; Zhang, C.; Liu, X.; Li, Q.; Xiong, M.; Zhang, Y.; Yin, S.; Ding, Y. Enhanced secondary organic aerosol formation during dust episodes by photochemical reactions in the winter in Wuhan. J. Environ. Sci. (uncorrected proof), **2022**; doi.org/10.1016/j.jes.2022.04.018

(26) Crowley, J.N.; Ammann, M.; Cox, R.A.; Hynes, R.G.; Jenkin, M.E.; Mellouki, A.; Rossi, M.J.; Troe, J.; Wallington, T.J.: Evaluated kinetic and photochemical data for Atmospheric Chemistry: Volume V – heterogeneous reactions on solid substrates, *Atmos. Chem. Phys.* **2010**, *10*, 9059-9223; doi.org/10.5194/acp-10-9059-2010

(27) Lederer, M.L.; Staniec, A.R.; Coates, Z.L.; Van Ry, D.A.; Hinrichs, R.Z. Heterogeneous Reactions of Limonene on Mineral Dust: Impacts of Adsorbed Water and Nitric Acid. *J. Phys. Chem. A* **2016**, *120*, 9545-9556; doi: 10.1021/acs.jpca.6b09865

(28) Niu, H; Chu B.; Su, W. ; Li, J. Heterogeneous Reactions between Toluene and NO_2 on Mineral Particles under Simulated Atmospheric Conditions. *Environ. Sci. & Technol*. **2017**, *51*, 9596-9604; doi: 10.1021/acs.est.7b00194

(29) Iannarelli, R.; Ludwig, C.; Rossi, M.J. Flowing Gas Experiments Reveal Mechanistic Details of Interfacial Reactions on a Molecular Level at Knudsen Flow Conditions. *Front. Astron. Space Sci*., 23 June **2022** | doi.org/10.3389/fspas.2022.891177

(30) Morris, M.A.; Bowker, M.; King, D.A. Kinetics of adsorption, desorption and diffusion at metal surfaces, chapter 1 in Comprehensive Chemical Kinetics, C.H. Bamford, C.F.H. Tipper and R.G. Compton, Vol. 19 (Simple Processes at the Gas-Solid Interface), Elsevier, **1984**.

(31) Suhasaria, T.; Thrower, J.D.; Zacharias, H. Thermal desorption of ammonia from crystalline forsterite surfaces. *Monthly Notices of the Royal Astronomical Society MNRAS* **2015**, *454*, 3317-3327

(32) Suhasaria, T.; Thrower, J.D.; Zacharias, H. Thermal desorption of astrophysically relevant molecules from forsterite (010). *Monthly Notices of the Royal Astronomical Society MNRAS* **2017**, *472*, 389-399

(33) Keyser, L.F.; Moore, S.B.; Leu, M.-T. Surface Reaction and Pore Diffusion in a Flow Tube Reactor, *J. Phys. Chem.* **1991**, *95*, 5496-5502

(34) Fenter, F.F.; Caloz, F.; Rossi, M.J. Kinetics of Uptake of HNO_3 on salt. *J. Phys. Chem.* **1994**, *98,* 9801-9810

(35) Komadel, P.; Madejová, J. Acid Activation of Clay Minerals. *Dev. Clay Sci*. **2013**, *5*, 385−408

(36) Oliveira, P.; Rojas-Cervantes, M.L.; Ramos, A.M.; Fonseca, I.M.; do Rego, A.M.B.; Vital, J. Limonene Oxidation over V_2O_5/TiO_2 Catalysts. *Catal. Today* **2006**, *118*, 307−314

(37) Yadav, M.K.; Patil, M.V.; Jasra, R.V. Acetoxylation and Hydration of Limonene and α-Pinene using Cation-Exchanged Zeolite Beta. *J. Mol. Catal. A: Chem*. **2009**, *297*, 101−109

(38) Comelli, N.; Avila, M. C.; Volzone, C.; Ponzi, M. Hydration of α-Pinene Catalyzed by Acid Clays. *Cent. Eur. J. Chem*. **2013**, *11*, 689− 697

(39) Mirghaffari, N. ; Iannarelli, R.; Ludwig, C.; Rossi, M.J. Coexistence of reactive functional groups at the interface of a powdered activated amorphous carbon: a molecular view. Molecular Physics, DOI: 10.1080/00268976.2021.1966110; September **2021** https://doi.org/10.1080/00268976.2021.1966110

(40) Chen, H, Li, Q., Wang, M., Ji, D. and Tan, W. XPS and two-dimensional FTIR correlation analysis on the binding characteristics of Humic acid onto Kaolinite surface, *Sci. Tot. Environ*. **2020**, *724,* 138154

(41) Kameda, T.; Azumi, E.; Fukushima, A.; Tang, N.; Matsuki, A., Kamiya, Y.; Toriba, A., Hayakawa, K. Mineral dust aerosols promote the formation of toxic nitropolycyclic aromatic compounds. *Sci. Rep.* **2016**, *6* (Nature Magazine), 24427; doi: 10.1038/srep24427 (2016)

(42) Esteve, W.; Budzinski, H.; Villenave, E. Relative rate constants for the heterogeneous reactions of OH, NO_2 and NO radicals with polycyclic aromatic hydrocarbons adsorbed on carbonaceous particles. Part 1: PAHs adsorbed on 1-2 µm calibrated graphite particles. *Atmos. Environ.* **2004**, *38*, 6063–6072

(43) Esteve, W.; Budzinski, H.; Villenave, E. Relative rate constants for the heterogeneous reactions of NO_2 and OH radicals with polycyclic aromatic hydrocarbons adsorbed on carbonaceous particles. Part 2: PAHs adsorbed on diesel particulate exhaust SRM 1650a. *Atmos. Environ.* **2006**, *40*, 201–211

(44) Miet, K.; Le Menach, K.; Flaud; P. M.; Budzinski, H.; Villenave, E. Heterogeneous reactivity of pyrene and 1-nitropyrene with NO_2: Kinetics, product yields and mechanism. *Atmos. Environ.* **2009**, *43*, 837–843

(45) Nguyen, M.L.; Bedjanian, Y.; Guilloteau, A. Kinetics of the reactions of soot surface-bound polycyclic aromatic hydrocarbons with NO_2. *J. Atmos. Chem.* **2009**, *62*, 139–150

(46) International Agency for Research on Cancer. Diesel and Gasoline Engine Exhausts and Some Nitroarenes, IARC Monographs on the Evaluation of Carcinogenic Risks to Humans. Vol. *105* (International Agency for Research on Cancer, **2013**)

Tables and Figures

Table 1: Parameters of the four aperture Knudsen flow reactor used in this study.

Parameter	**Value**
Reactor Volume V	1830 cm^3
Estimated internal surface area A_v	1300 cm^2
Sample plate surface area A_s	10.6 cm^2
Escape orifice diameter (nominal Ø)	1, 4, 8 and 14 mm
Collision frequency [a] ω / s^{-1}	21.0 $(T/M)^{1/2}$
Collision Frequency per cm^2 of surface/s^{-1}	1.98 $(T/M)^{1/2}$
Escape rate constants k_e [b]/s^{-1}	
1 mm orifice	0.0149 $(T/M)^{1/2}$
4 mm orifice	0.213 $(T/M)^{1/2}$
8 mm orifice	0.763 $(T/M)^{1/2}$
14 mm orifice	1.827 $(T/M)^{1/2}$

[a]Calculated based on the geometric surface area of the Pyrex sample cup (10.6 cm^2) placed in the 50 mm diameter and 50 mm high sample compartment. Please take note of variable surface areas listed in Table 3

[b]Experimentally determined using Ozone, SO_2 and $CHCl_3$. T is temperature (K) and M is molecular mass (g mol^{-1}); k_e is the effusion rate constant in s^{-1}

Table 2 : Representative uptake data on semivolatile hydrocarbons and H_2O interacting with Kaolinite LO and Arizona Test Dust (ATD) Coarse measured in the 1 mm Ø orifice KFR.

Semivolatile probe gas	**Experiment #**	**Solid Substrate**	**ML to saturation %ML**	**Prompt Desorption % saturation**	**Readsorption post pumping[c] %**	**Adsorbate persisting in % after pumping[c]**	**Adsorbate[f] pumped overnight (≥15 h) in %**
Applinate	FS40/41[a]	ATD Coarse	25.3	10.0	34.6	65.4	24.6
Applinate	FS10/11	Kaolinite LO	9.6	60.0	91.0	9.0	31.0
Pipol	FS90/91	ATD Coarse	(100.0)[e] 116.8	13.4	24.7	75.3	11.3
Pipol	FS100/101	Kaolinite LO	49.0	24.6	62.0	38.0	37.4
Menthol	FS60/61[b]	ATD Coarse	10.9	3.4	12.3	88.7	8.9
Menthol	FS70/71	Kaolinite LO	4.9	26.9	63.9	36.1	37.0
Benzylacetate[d]	S203/204	ATD Coarse	16.9	23.6	38.1	61.9	**14.5**
Benzylacetate[d]	S205/206	Kaolinite LO	14.1	53.1	63.2	36.8	**10.1**
Limonene	S207/208	ATD Coarse	10.2	No des.	20.2	79.8	20.2
Limonene	S209/210	Kaolinite LO	40.8	No des.	29.1	69.9	29.1
γ-Terpinene	S214/S215	ATD Coarse	7.5	8.7	22.0	78.0	13.3
γ-Terpinene	S216/S217	Kaolinite LO	12.2	6.9	26.5	73.5	19.6
Toluene	S218/S19	ATD Coarse	11.2	50.8	65.0	35.0	14.2
Toluene	S221/S223	Kaolinite LO	3.3	58.0	87.5	12.5	29.5
H_2O	S246/S247	ATD Coarse	21.1	> 79.2[g]	109.3 (100.0)	0.0	0.0
H_2O	S243	Kaolinite LO	7.9	100.0	100.0	0.0	0.0

[a] After desorption 90% of all sites are still occupied. After pumping the whole night in the 14 mm orifice reactor re-adsorption of applinate at 34.6% leaves 100-34.6 = 65.4% of all sites occupied from the previous experiment. Therefore, overnight pumping removed 90-65.4 = 24.6% of applinate molecules

[b] Unlike all other samples it was pumped for 70 h over a long weekend so that value must be regarded as an upper limit

[c] Sum of columns 6 and 7 is 100%

[d] Uptake on empty KFR is 1.33 10^{17} molecule

[e] Arbitrarily set to 100% rather than using the estimate for a molecular monolayer (that is given in small print below the notion of 100%)
[f] Corresponds to the difference between values in column 6 minus column 5
[g] Lower limiting value, may be 100%

Table 3: Kinetic Data for adsorption (k_a) and desorption (k_d) of semivolatiles and H_2O interacting with Kaolinite LO and Arizona Test Dust Coarse (ATD-C) in the 1 mm Ø orifice [a]

Min Dust Material	**Semi-volatile**	**k_e / s^{-1}**	**k_0 / s^{-1}**	**k_a / s^{-1}**	**k_d / s^{-1}**	**1 / k_d**	**Exp. #**
ATD Coarse	Applinate	0.0215	1.45-4.43	2.0	$4.0\ 10^{-5}$	25’000	FS40
Kaolinite LO	Applinate	0.0215	1.36-4.08	4.0	$1.5\ 10^{-4}$	6’700	FS10
ATD Coarse	Pipol	0.0216	0.232	0.90	$3.0\ 10^{-4}$	3’300	FS90
Kaolinite LO	Pipol	0.0216	1.074	1.70	$3.0\ 10^{-4}$	3’300	FS100
ATD Coarse	Menthol	0.0207	0.346	0.35	$2.5\ 10^{-5}$	40’000	FS60
Kaolinite LO	Menthol	0.0207	0.489	0.50	$7.0\ 10^{-5}$	14’300	FS70
ATD Coarse	Benzylacetate	0.0211	0.083	8.0	$8.0\ 10^{-6}$	125’000	S203
ATD Coarse	Benzylacetate	0.0211	0.190	1.3	$8.0\ 10^{-5}$	12’500	S238
Kaolinite LO	Benzylacetate	0.0211	> 2.0	4.5	$3.0\ 10^{-5}$	33’300	S239
Kaolinite LO	Toluene	0.0269	0.0572	1.3	$3.0\ 10^{-3}$	333	S240
ATD Coarse	Toluene	0.0269	0.0802	2.5	$2.0\ 10^{-2}$	50	S241
Kaolinite LO	H_2O	0.0609	1.42	3.0	$5.0\ 10^{-4}$	2000	S242
Kaolinite LO	H_2O	0.0609	0.465	3.0	$3.0\ 10^{-4}$	3330	S243
ATD Coarse	H_2O	0.0609	1.082	2.0	$3.0\ 10^{-4}$	3330	S246
ATD Coarse	H_2O	0.0609	0.88	2.0	$3.0\ 10^{-4}$	3330	S247

[a] sample surface area is 10.6 cm^2 corresponding to diameter of Pyrex sample cup

Table 4 : Kinetic Data: initial uptake coefficients γ_0 based on k_0 (initial adsorption rate constant) and geometric surface area[a,b,d]

Sample ID	Mass/ mg	Organics	Substrate	Geom. Surface/cm^2	14 mm Ø[d] γ_0	8 mm Ø γ_0	4 mm Ø γ_0	1 mm Ø γ_0
S224	11.4	Limonene[b]	Kaolinite LO	0.292	**0.260**	0.191	0.0646	not det.
S230	73.2	Limonene	ATD C	1.131	**0.249** **(0.131)**	0.156	0.103	0.0445
S231	36.6	Limonene[c]	Kaolinite LO	1.131	**0.633** **(0.302)**	0.511	0.452	0.220
S225	40.8	Toluene	Kaolinite LO	1.131	**0.049**	0.014	not det.	$3.7\ 10^{-3}$
S226	91.0	Toluene	ATD C	1.131	**0.091**	0.041	0.025	$9.0\ 10^{-3}$
S227	54.3	γ-Terpinene	Kaolinite LO	1.131	**0.434**	0.0117	0.054	$5.5\ 10^{-3}$
S232	52.9	γ-Terpinene	ATD-C	1.131	**0.302** **0.245**[e] **(0.199)**	0.153	0.0768	0.0151
S233	55.5	Applinate	ATD-C	1.131	**0.648** **(0.353)**	0.316	0.166	0.0261
S234	45.1	Applinate	Kaolinite LO	1.131	**0.767** **(0.365; 0.290)**	0.252	0.250	0.0607
S235	52.4	Benzylacetate	Kaolinite LO	1.131	**0.683** **(0.280)**	0.331	0.163	0.0318
S237	52.4	Benzylacetate	ATD-C	1.131	**0.364; 0.316** **(0.105)**	0.226 (0.121)	0.129 (0.057)	0.0234

[a] Same sample measured back-to-back starting with 14 mm Ø diameter orifice size (multiple exposure)

[b] Throughout the kinetics series the geometric surface area was 1.131 cm^2 except for S224 Limonene/Kaolinite LO) where it was 0.292 cm^2

[c] Formal values for γ for 14, 8 and 4 mm Ø orifices are 0.633, 0.522 and 0.450, respectively

[d] Small numbers in brackets correspond to repeat experiments after going through the orifice sequence 14, 8, 4 and 1 mm Ø using the same solid substrate. See Figures 6 and 7

[e] Corresponds to the second exposure immediately after the first at 14 mm orifice Ø at a selected low flow rate

Figures

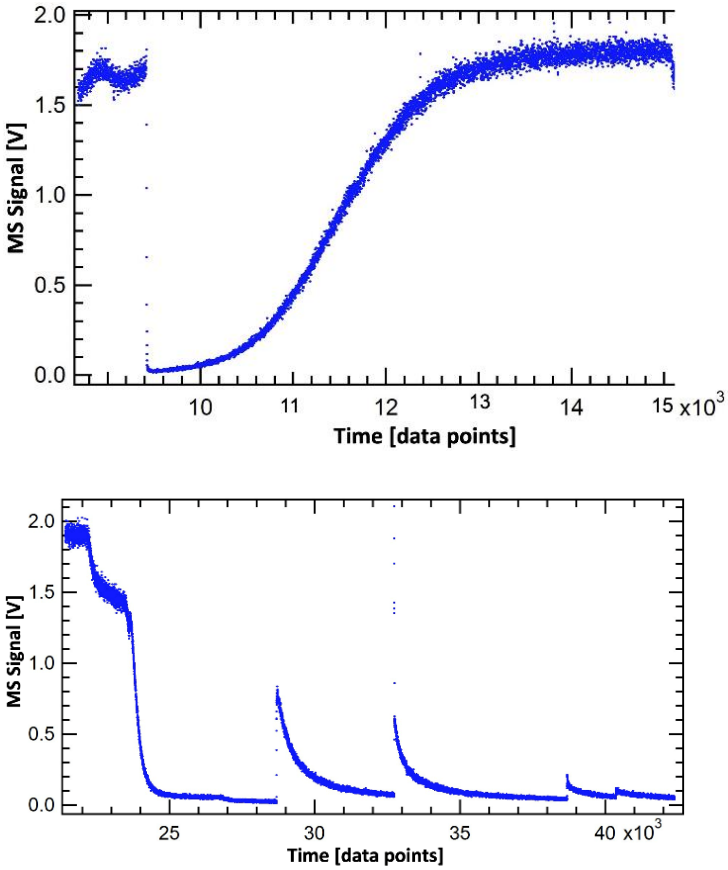

Figure 1a (upper panel) and 1b (lower panel): Applinate heterogeneous interaction (experiment FS10, Kaolinite LO): raw data of uptake phase (upper panel) at F^i = 3.1 10^{15} molecule s^{-1}, (spontaneous) desorption phase (lower panel); ordinate: MS signal in V (Lock-in amplifier) monitored at 102 amu; abscissa: points (recording frequency of 4 s^{-1}). The four desorption traces starting at 29'000 pts. in the lower panel correspond to (nominal) 14, 8, 4 and 1 mm diameter orifice reactors. See Table 2 and 3 for quantitative desorption data.

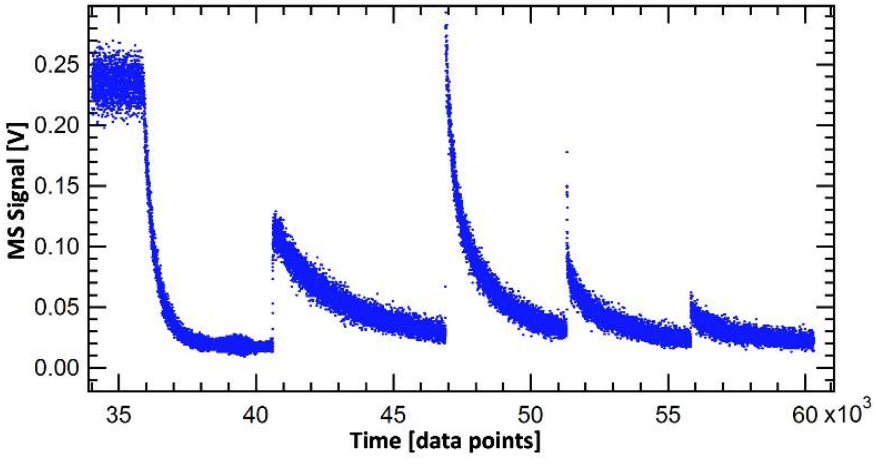

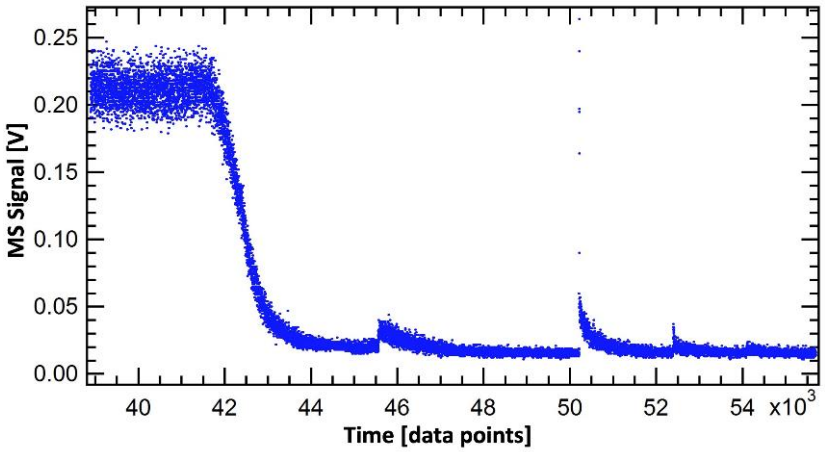

Figure 2a (upper panel) and 2b (lower panel): Desorption experiments at ambient temperature for menthol (detected at 81 amu) on Kaolinite LO (upper panel, FS70/71: F^i = 5.6 10^{13} molecule s^{-1}) and ATD Coarse (lower panel, FS60/61: F^i = 7.6 10^{13} molecule s^{-1}) at 1, 4, 8 and 14 mm orifice diameter starting at 41'000 and 45'000 pts, respectively (data recording frequency of 4 pts s^{-1}). The ordinate represents the lock-in amplifier signal in V. See Table 2 and 3 for quantitative desorption data.

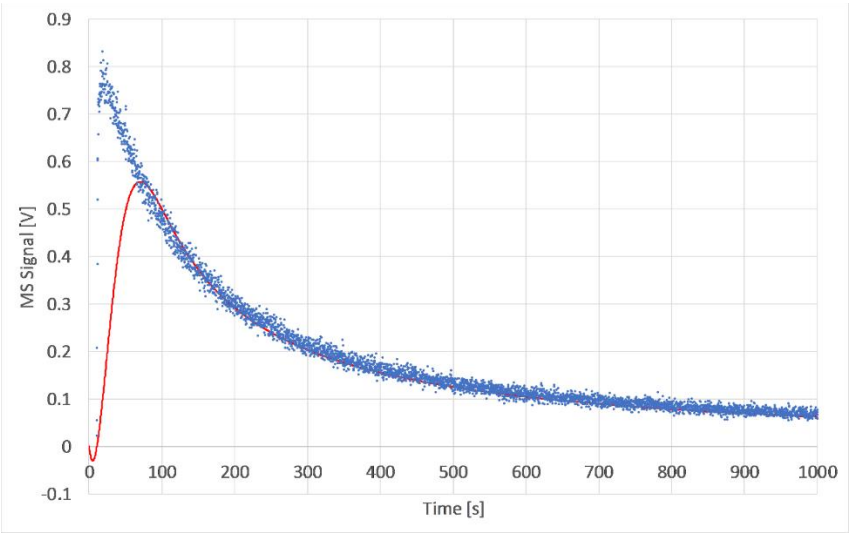

Figure 3: Desorption fit for applinate/Kaolinite LO (FS10) monitored at 102 amu in the 1 mm Ø orifice KFR, k_d = 1.4 10^{-4}; k_a = 4.0; k_e = 0.0215 s^{-1} whose uptake phase is given in Figure 1 above. See Table 3 for quantitative data.

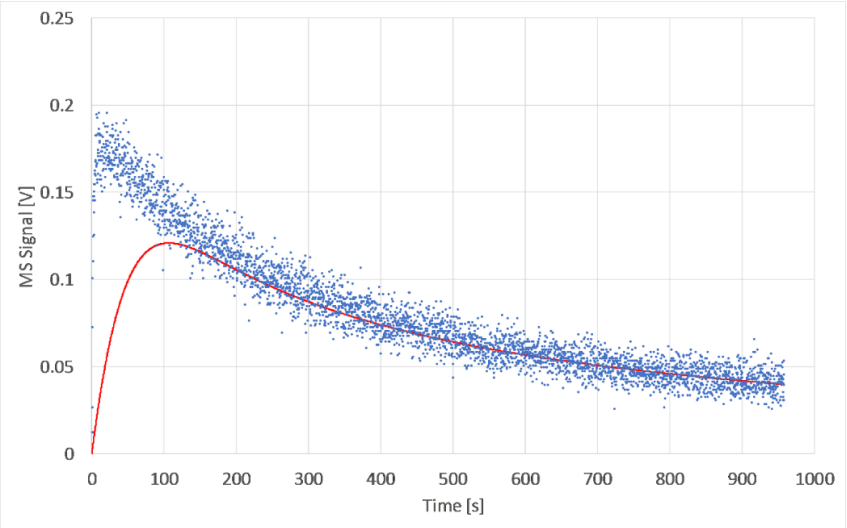

Figure 4: Desorption fit for applinate/ATD Coarse (experiment FS40) in the 1 mm Ø orifice KFR monitored at 102 amu with k_d = 4.0 10^{-5}; k_a = 2.0, k_e = 0.0215 s^{-1}. See Table 3 for quantitative data.

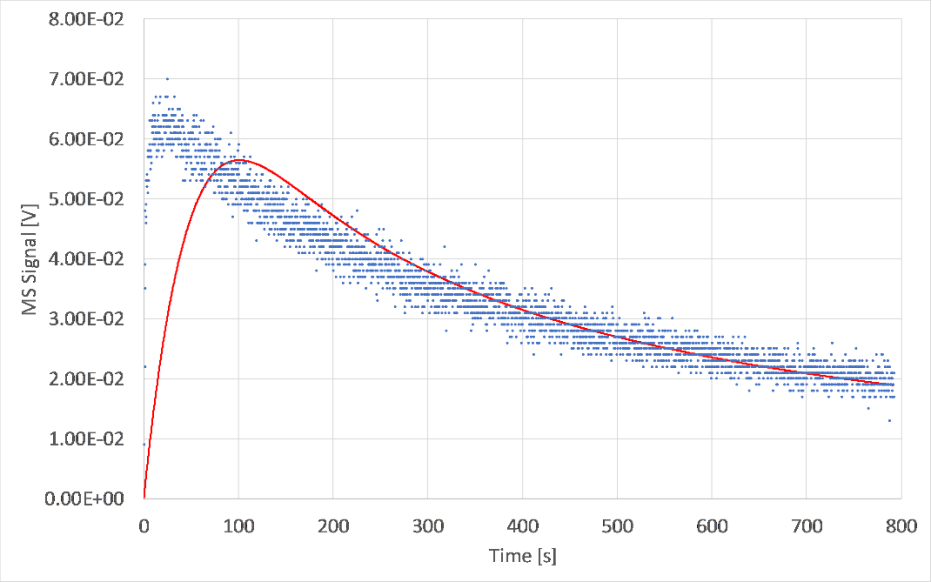

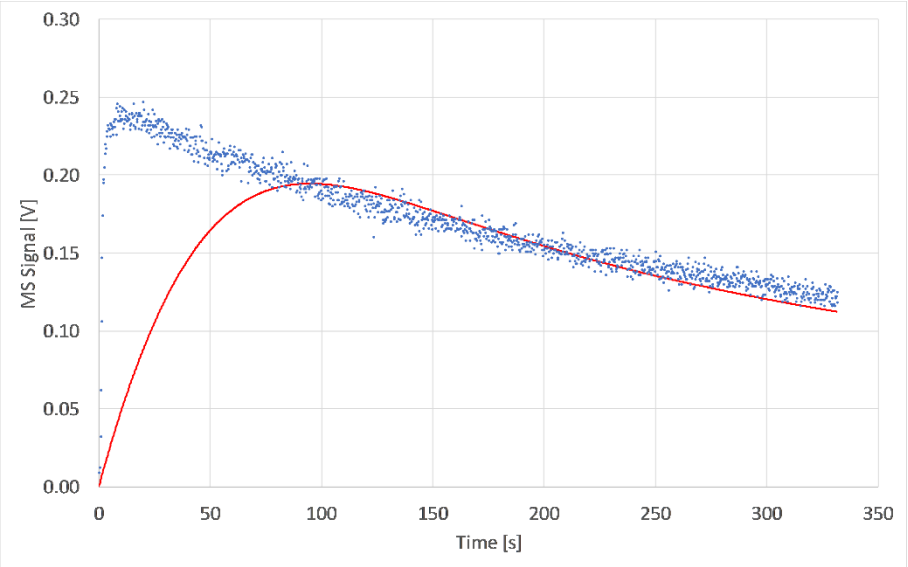

Figure 5a (upper panel) and 5b (lower panel): Benzylacetate desorption monitored at 108.1 amu. Upper panel: 51.9 mg ATD-C in 1 mm Ø KFR (experiment S238; k_d = 8.0 10^{-5}, k_a = 1.3, k_e = 0.0211 s^{-1}); Lower panel: 55.3 mg Kaolinite LO in 1 mm Ø KFR (experiment S239; k_d = 3.0 10^{-5}, k_a = 4.5, k_e = 0.0211 s^{-1}). See Table 3 for quantitative data.

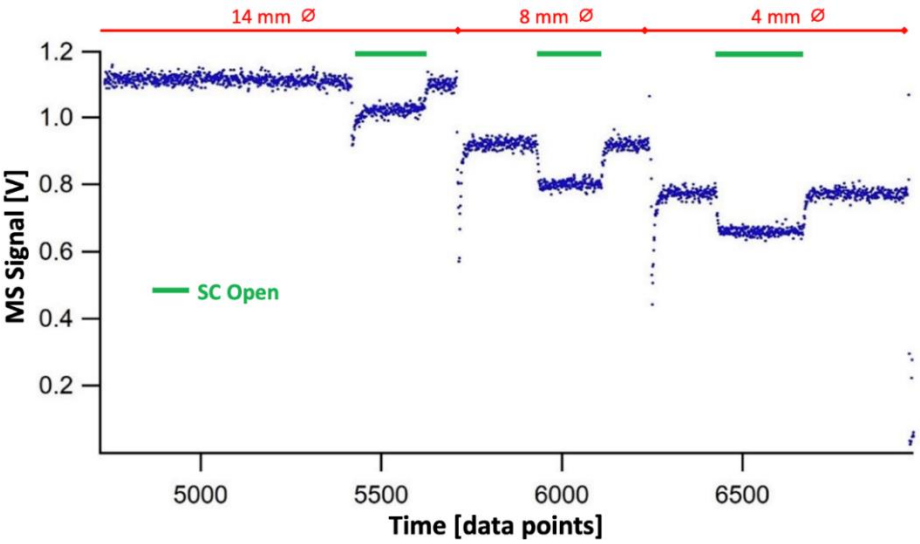

Figure 6: Experiment S224 (Limonene/Kaolinite LO) at a constant flow rate F^i = 3.81 10^{14} molecule s^{-1}. Red labels correspond to KFR exit orifice diameter. The downward spikes are due to filling of the SC when recording the uptake kinetics successively from 14 to 8 to 4 mm diameter orifices with increasing concentration at 5500, 6000 and 6500 points, respectively. The uptake probability has been evaluated using the horizontal portion of the MS signal after opening the SC. See Table 4 for quantitative data.

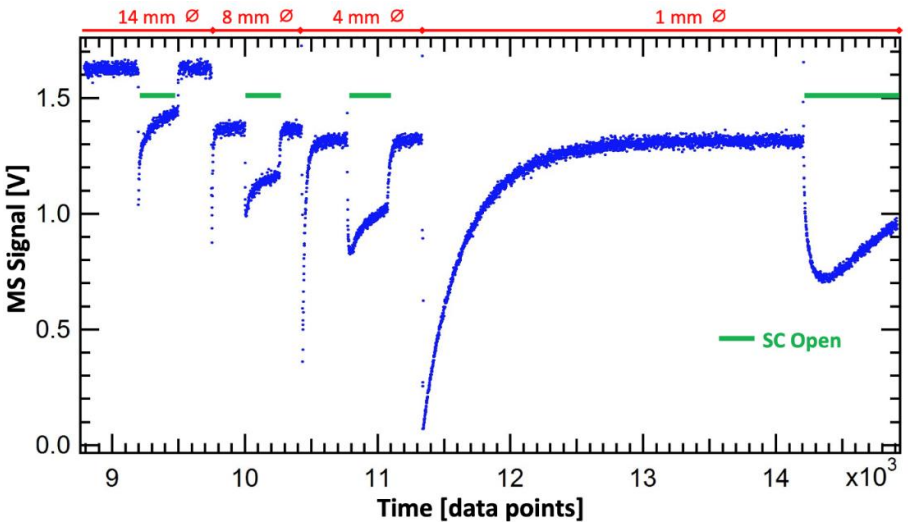

Figure 7: Experiment S227 (γ-Terpinene/Kaolinite LO) at a constant flow rate F^i = 7.71 10^{14} molecule s^{-1} starting with 14 mm Ø orifice at 9000 pts. Red labels correspond to KFR exit orifice diameter. Initial uptake recorded at 9'200, 10'000, 10'300 and 14'200 pts. For 14, 8, 4 and 1 mm Ø orifice, respectively. Additional explanations given in caption of Figure 5. See Table 4 for quantitative data.

Scheme I

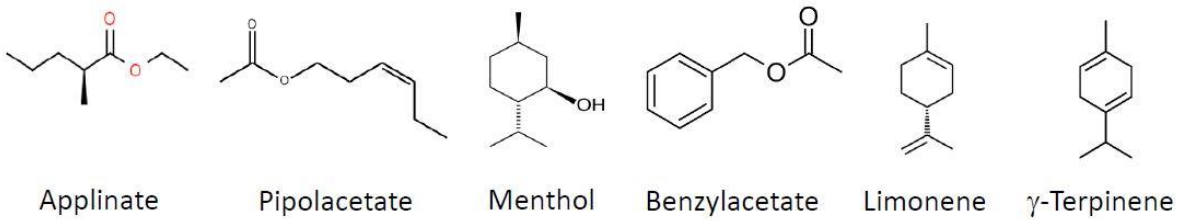

Scheme I (optional)

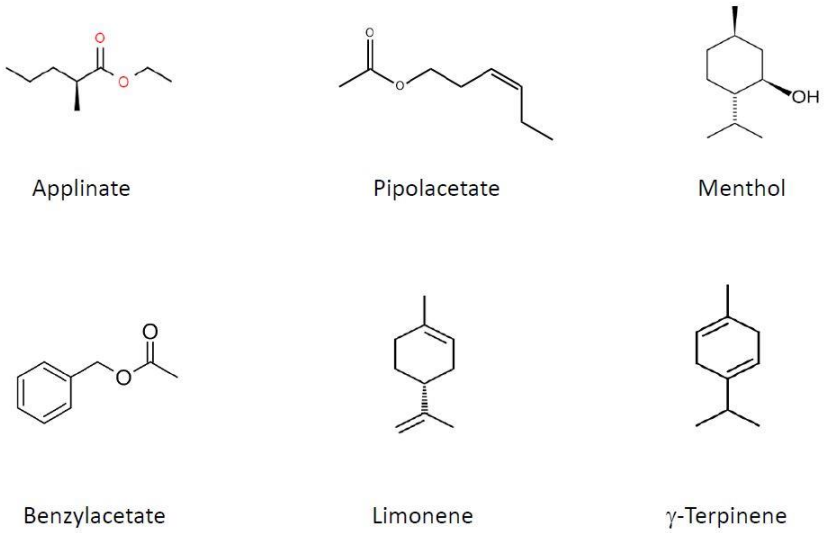

Graphical Abstract: